

# Encapsulation of Perchlorate Salts within Metal Oxides for Application as Nanoenergetic Oxidizers

Chunwei Wu, Kyle Sullivan, Snehaunshu Chowdhury, Guoqiang Jian, Lei Zhou, and Michael R. Zachariah\*

In this work, high-oxygen-content strong oxidizer perchlorate salts were successfully incorporated into current nanothermite composite formulations. The perchlorates were encapsulated within mild oxidizer particles through a series of thermal decomposition, melting, phase segregation, and recrystallization processes, which occurred within confined aerosol droplets. This approach enables the use of hygroscopic materials by stabilizing them within a matrix. Several samples, including  $\text{Fe}_2\text{O}_3/\text{KClO}_4$ ,  $\text{CuO}/\text{KClO}_4$  and  $\text{Fe}_2\text{O}_3/\text{NH}_4\text{ClO}_4$  composite oxidizer particles, have been created. The results show that these composite systems significantly outperform the single metal oxide system in both pressurization rate and peak pressure. The ignition temperatures for these mixtures are significantly lower than those of the metal oxides alone, and time-resolved mass spectrometry shows that  $\text{O}_2$  release from the oxidizer also occurs at a lower temperature and with high flux. The results are consistent with  $\text{O}_2$  release being the controlling factor in determining the ignition temperature. High-speed imaging clearly shows a much more violent reaction. The results suggest that a strategy of encapsulating a very strong oxidizer, which may not be environmentally compatible, within a more stable weak oxidizer offers the opportunity to both tune reactivity and employ materials that previously could not be considered.

nanoscale constituents that enable intimate mixing of the fuel and oxide, whose nanodimensional homogeneity results in substantial enhancement in heat and mass diffusion, and therefore in reactivity and burn rate.<sup>[3–5]</sup> It has been experimentally observed that the activation energy for nanoaluminum oxidization and for the oxidizer decomposition is significantly lower than the corresponding values for their macroscopic counterparts,<sup>[6]</sup> and the higher surface area of nanoaluminum presumably is at least partially responsible for the higher reaction rate and facilitates energy transfer.<sup>[7]</sup> Aumann et al. were some of the first to see the enhanced performance that nanoenergetic materials could potentially deliver, with a 1000 x increase in reactivity.<sup>[8]</sup> It has been speculated that this increase in reaction-propagation rate is related to the mode of energy transfer in a composite, which likely shifts from conductive to convective mode.<sup>[9,10]</sup> These results have been confirmed by further studies by others who have shown that the packing density is inversely correlated with reaction velocity and that intimacy of mixing is a key variable.<sup>[11]</sup>

## 1. Introduction

Nanothermite, a subset of metastable intermolecular composites (MIC), is a relatively new class of energetic materials (EMs) that is finding applications in propellants and explosives, as well as microscale energetic material applications and microelectromechanical systems (MEMS).<sup>[1,2]</sup> These solid-state redox reaction systems have in common very rapid, exothermic and self-propagating behavior. With respect to traditional inorganic solid-state EMs, which are a mixture of fine powders of oxidizer and reducing agent, nanothermite is characterized by

This latter point suggests that the manner of assembling the fuel and oxidizer either through physical mixing, or through direct assembly and microstructure manipulation, may yield new and more controllable properties. This approach has led to, for example, self-assembled  $\text{Al}/\text{Fe}_2\text{O}_3$  nanotubes,<sup>[7]</sup> self-assembled  $\text{Al}/\text{CuO}$  nanorods,<sup>[12,13]</sup> nanowired  $\text{Al}/\text{CuO}$ ,<sup>[2,14]</sup> electrostatically assembled  $\text{Al}/\text{Fe}_2\text{O}_3$  nanoparticles,<sup>[15]</sup> and  $\text{Al}/\text{SnO}_2$  coating by atomic layer deposition (ALD).<sup>[16]</sup>

While there is a wide variety of possible metal and oxidizer combinations for thermite mixtures, aluminum (Al) is most often the fuel choice, due to its availability, high reaction enthalpy, low ignition temperature, high thermal conductivity, and the passivation nature of its native oxide. Furthermore, the high negative enthalpy of the oxide of aluminum ( $\text{Al}_2\text{O}_3$ ) offers many possible low-cost metal oxides as possible oxidizers, including  $\text{Fe}_2\text{O}_3$ ,  $\text{CuO}$ ,  $\text{MoO}_3$ ,  $\text{Bi}_2\text{O}_3$ ,  $\text{WO}_3$ , and  $\text{SnO}_2$ , etc.<sup>[1,17,18]</sup>

On the other hand, one can envision many other more powerful oxidizer molecules; many of these are typically composed of salts. For example, ammonium perchlorate (AP) is a very labile species composed of the perchlorate ion  $\text{ClO}_4^-$ , with

Dr. C. Wu, K. Sullivan, S. Chowdhury, L. Zhou, Prof. M. R. Zachariah  
Department of Mechanical Engineering  
University of Maryland  
College Park, MD 20742, USA  
E-mail: mrz@umd.edu

G. Jian, M. R. Zachariah  
Department of Chemistry and Biochemistry  
University of Maryland  
College Park, MD 20742, USA



DOI: 10.1002/adfm.201100479

chlorine in an oxidation state of +7. The high oxygen content and good thermal stability of perchlorates have made them indispensable ingredients for the pyrotechnics industry and as key ingredients in solid rocket propellants. For example, composite solid rocket propellants typically contain 60 wt%–80 wt% ammonium perchlorate (AP), together with a polymer binder [e.g., polybutadiene acrylic acid acrylonitril terpolymer (PBAN), hydroxyl-terminated polybutadiene (HTPB), nitramines, tetrazoles, and nitrourethanes] and metallic fuel like aluminum powder.<sup>[19]</sup> In microscale MEMS applications, perchlorates such as  $\text{Ca}(\text{ClO}_4)_2$ ,  $\text{KClO}_4$  and  $\text{NaClO}_4$  have been incorporated into nanoporous silicon by impregnation or a vapor deposition technique.<sup>[1,20]</sup> Among the various perchlorate salts, AP is the most widely used today as it yields high heat and high oxygen content. Potassium perchlorate (PP) is also a good solid propellant additive because of its fast burn rate and high caloric value.

Unfortunately, these oxidizers have not found application in MIC formulations due to their highly hygroscopic nature, which poses long-term stability constraints on the nanofuel (e.g., aluminum). Perchlorate release, due to its water solubility, has raised many environmental concerns during manufacture, transport, and launch operations.<sup>[21]</sup>

Ideally one would like to harness the oxidizer properties of perchlorates, with the longevity and stability offered by traditional metal oxides. Herein we focus on developing a generic strategy of encapsulation of the strong oxidizer within a relatively mild and insoluble oxidizer. This strategy was previously tested by us in the fabrication of a core-shell-structured  $\text{Fe}_2\text{O}_3/\text{KMnO}_4$  which showed enhanced performance characteristics.<sup>[22]</sup> In the current work, we describe a generic method to produce composite-structure oxidizer particles, with several powerful oxidizer perchlorates being successfully encapsulated within common inorganic oxides such as  $\text{Fe}_2\text{O}_3$  and  $\text{CuO}$ . The synthesis is realized via an aerosol-based spray drying/pyrolysis method, by employing careful control of the

precursor-decomposition and melting processes. The aerosol technique enables formation of nanosized perchlorate particles via a process of recrystallization out of solution phase within an aerosol droplet, and simultaneous encapsulation of each perchlorate particle with an oxide shell, which is derived from the thermal decomposition of a metal nitrate precursor. The resulting materials are tested for their combustion behavior and compared with existing formulations.

## 2. Results and Discussion

### 2.1. Synthesis of $\text{Fe}_2\text{O}_3/\text{KClO}_4$ , $\text{CuO}/\text{KClO}_4$ and $\text{Fe}_2\text{O}_3/\text{NH}_4\text{ClO}_4$ Composite Oxidizer

Microstructure control of the composite particles was realized by tuning the temperatures of the two furnaces that govern the thermal decomposition of the metal nitrates and the melting of the perchlorate. In a typical synthesis (e.g.,  $\text{Fe}_2\text{O}_3/\text{KClO}_4$ ), a precursor aqueous solution of iron (III) nonahydrate and potassium perchlorate was sprayed into aerosol droplets by an atomizer. The molar ratio of the starting component salts Fe/K was fixed at 1:2, and the total salt precursor concentration was kept constant at 5.0 wt%. The temperature of the first furnace ( $T_1$ ) was set at 125 °C and the second ( $T_2$ ) at 550 °C.

Before or just entering the first furnace, water evaporation from the droplet drives the crystallization or precipitation of both iron nitrate and potassium perchlorate. Each aerosol droplet may be considered as a microreactor containing a solid mixture of the two starting component salts. In the first furnace, iron nitrate ( $T_{\text{decomp}}(\text{Fe}(\text{NO}_3)_3) = 125$  °C) decomposes to form iron oxide while potassium perchlorate ( $T_{\text{m.p.}}(\text{KClO}_4) = 525$  °C) remains a solid. From the TEM image in **Figure 1** one can clearly see the distinct core-shell morphology. This structure

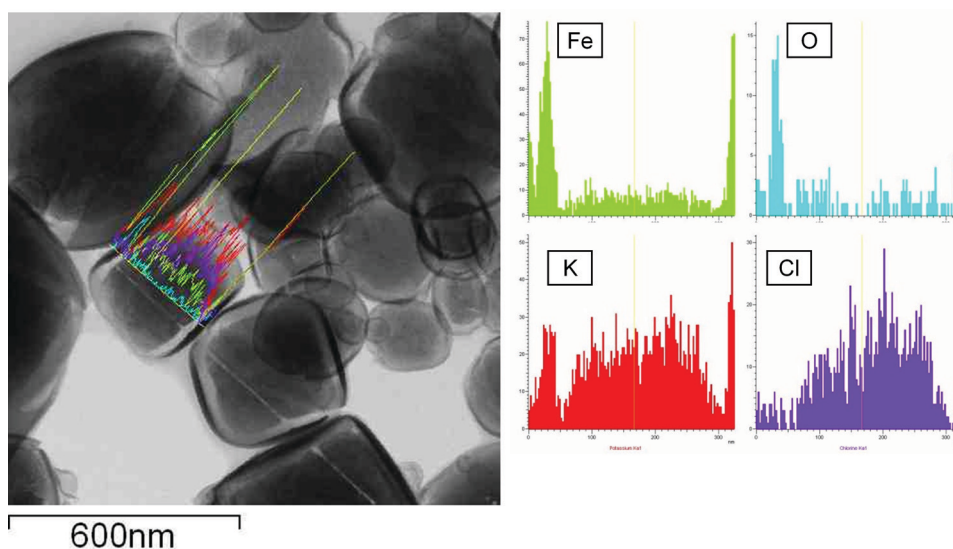


**Figure 1.** TEM image (left) and EDS line scan analysis (right) of the composite  $\text{Fe}_2\text{O}_3/\text{KClO}_4$  particles, revealing the elemental concentration profile of Fe, O, K and Cl across the line,  $[\text{Fe}/\text{K}] = \frac{1}{2}$  in precursor solution.

was confirmed by use of EDS line-scan analysis (Figure 1) to identify the elemental profile of Fe, O, K, and Cl along the selected line across the particles. Quite clearly we have created a structure of a very strong oxidizer encapsulated within a weak oxidizer shell.

While the mechanism of formation is unknown, we can speculate on likely routes. In one case the drying droplet results in a homogeneously dispersed solid particle containing the two precursors. In the first furnace thermal decomposition of the iron precursor leads to small iron oxide clusters within the solid  $\text{KClO}_4$  matrix. As the temperature is raised to the melting point of  $\text{KClO}_4$ , i.e., in the second furnace, the solid matrix becomes molten and liquidlike. At this point the iron oxide clusters become mobile, and begin to aggregate and coalesce at the exterior of the aerosol particle due to surface-tension forces. As the particles cool down, the molten  $\text{KClO}_4$  recrystallizes to form a solid core that is encapsulated by the exterior oxide shell.

A second possibility is that the core-shell structure is created during the drying process and before the chemistry is initiated, which results in a core-shell  $\text{KClO}_4/\text{Fe}(\text{NO}_3)_3$  structure. However the perchlorate is about 80 times less soluble than the iron precursor (at room temperature), so one would expect that if this was occurring the perchlorate would be on the outside, where the evaporation of the solvent would cause the local concentration of the solute to be the highest and leading to precipitation of the least soluble component first. In either case it is clear from the figure that the perchlorate is in the interior, that a near perfect phase separation has occurred, and that crystallization of the perchlorate causes the shell to take on a non-spherical shape.

In order to clarify the microstructure formation mechanism, we conducted another similar experiment at lower temperatures, i.e.,  $T_1/T_2 = 90\text{ }^\circ\text{C}/90\text{ }^\circ\text{C}$ , in which no decomposition of iron nitrate or melting of perchlorate could occur. **Figure 2** exhibits the TEM image along with the EDS analysis of

the derived particles. It is quite clear that a core-shell structure is formed during the drying/precipitation. However, in this case considerably more iron can be found within the core of the particles and less potassium than in the previous case. This result suggests that, despite the lower solubility of the perchlorate, a net phase-separation process occurs during the droplet evaporation process that creates the core-shell structure. Apparently heating the particle to create the oxide and then subsequently melt the perchlorate serves to further drive the phase-separation process.

The copper oxide/potassium perchlorate ( $\text{CuO}/\text{KClO}_4$ ) composite structure shown in **Figure 3**, was obtained at  $T_1/T_2 = 400\text{ }^\circ\text{C}/550\text{ }^\circ\text{C}$ . As in the iron example, the choice of temperatures was governed by the decomposition and melting points. In this example, as before, the nitrate has a much higher solubility than the perchlorate. While the structure is obviously core-shell, crystallization of the perchlorate has clearly been disrupted. Careful examination of the TEM image reveals small  $\text{CuO}$  crystallites dispersed throughout, which could result from the incomplete coalescence and aggregation of  $\text{CuO}$  primary particles from the molten  $\text{KClO}_4$  matrix. Possibly this result is because in this case the reactor temperatures are very close to each other, due to the relatively high decomposition temperature of the copper precursor. So in this case the material can be best described as  $\text{CuO}$ -rich shell composite.

The influence of phase segregation on morphology is even more prominent for the iron oxide/ammonium perchlorate ( $[\text{Fe}_2\text{O}_3/\text{NH}_4\text{ClO}_4]$ ) system, which was experimentally achieved with  $T_1/T_2 = 125\text{ }^\circ\text{C}/200\text{ }^\circ\text{C}$  and is shown in **Figure 4**. EDS analysis indicates that the two components form a homogeneous hollow shell. In this case both components behave similarly as under conditions seen for spray pyrolysis, in which solvent evaporation from the droplet leads to a hollow structure. In our case the two solutes have solubilities that are similar (ca. sixfold difference at room temperature).

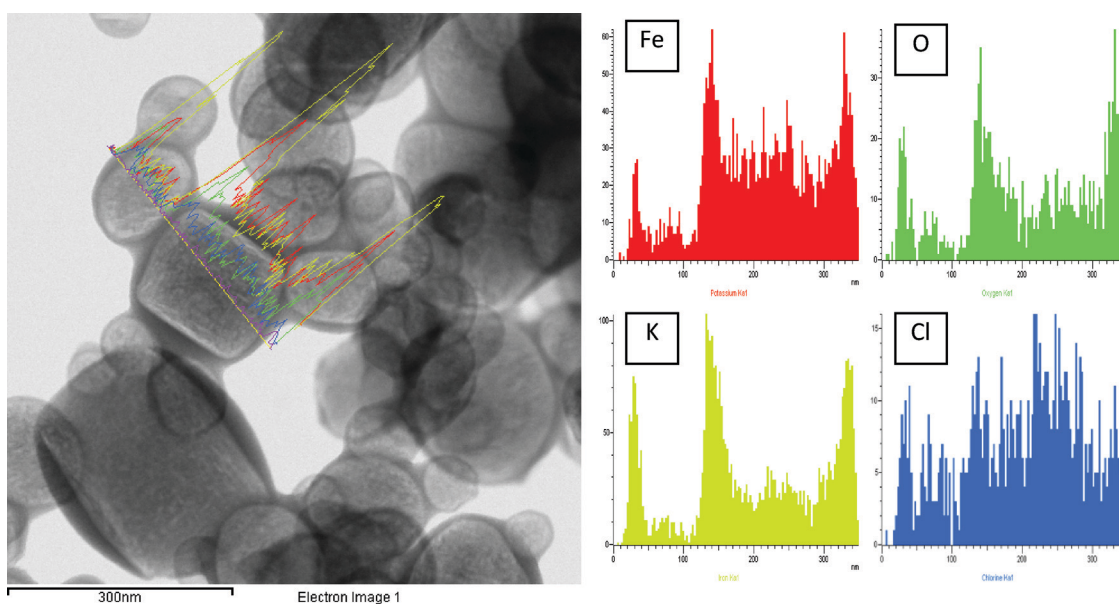


**Figure 2.** TEM image (left) and EDS line-scan analysis (right) of the composite  $\text{Fe}_2\text{O}_3/\text{KClO}_4$  particles obtained at  $T_1/T_2 = 90\text{ }^\circ\text{C}/90\text{ }^\circ\text{C}$ .

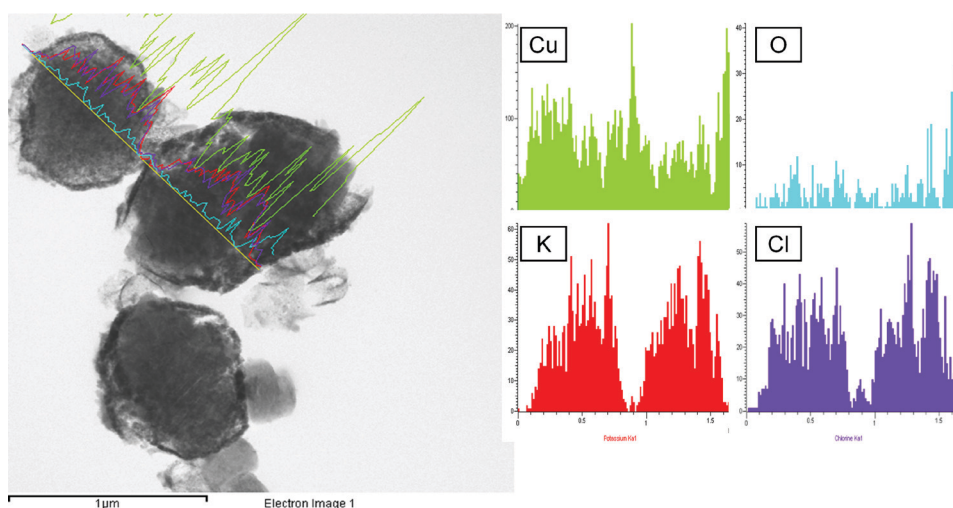


**Figure 3.** TEM image (left) and EDS line scan analysis (right) of the composite CuO/KClO<sub>4</sub> particles, revealing the elemental concentration profile of Cu, O, K, and Cl across the line, [Cu/K] = ½ in precursor solution.

## 2.2. Characterizations of Combustion Performance

The relative reactivity for stoichiometric (i.e., equivalence ratio  $\varphi = 1$ ) mixtures of nano-Al with the oxidizers was measured using the combustion cell. The pressure signals are shown for the various synthesized oxidizers in **Figure 5a** along with CuO nanopowder ( $\approx 50$  nm, Sigma-Aldrich) and Fe<sub>2</sub>O<sub>3</sub> nanopowder ( $< 50$  nm, Sigma-Aldrich) as reference materials. All systems except Fe<sub>2</sub>O<sub>3</sub> show a fast pressure rise which occurs on the order of microseconds. The perchlorate materials, however, exhibit much higher overpressures than the reference CuO (purple curve) and Fe<sub>2</sub>O<sub>3</sub> (light blue curve, barely seen on this scale). Another qualitative comparison is with the Al/Bi<sub>2</sub>O<sub>3</sub> system. Martirosyan et al.<sup>[23]</sup> demonstrated the highest pressure pulse for Al/Bi<sub>2</sub>O<sub>3</sub> among reported thermite reactions, which suggests that this extraordinary high pressure results from

evaporation of the combustion product Bi, whose boiling point is lower than the maximum reaction temperature. A pressurization rate of up to 650 GPa s<sup>-1</sup> ( $\approx 94.3$  psi  $\mu$ s<sup>-1</sup>) was shown in their study, which is considerably lower than that achieved in our materials, without considering the larger sample mass/cell volume ratio of their testing system (i.e., 500 mg/85 cm<sup>3</sup> vs. 25 mg/13 cm<sup>3</sup>). The peak pressure, rise time, and pressurization rate are summarized in **Table 1**.

The corresponding optical emission for the same systems is shown in **Figure 5b**. In this case, some obvious differences were seen for the various systems. The oxidizers containing CuO exhibited an intense optical rise and decay, whereas the oxidizers with Fe<sub>2</sub>O<sub>3</sub> showed a much weaker optical signal with a prolonged “tail”. In all cases, the timescale of optical emission was several hundred microseconds, much longer than the rise time of the pressure signal.

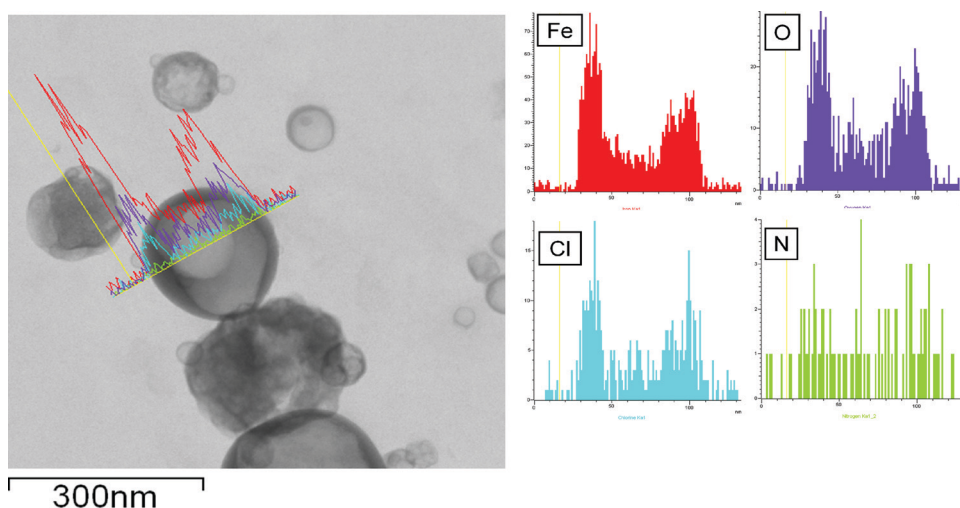


**Figure 4.** TEM image (left) and EDS line-scan analysis (right) of the composite Fe<sub>2</sub>O<sub>3</sub>/NH<sub>4</sub>ClO<sub>4</sub> particles, revealing the elemental concentration profile of Fe, O, N, and Cl across the line, [Fe/N] = ½ in precursor solution.

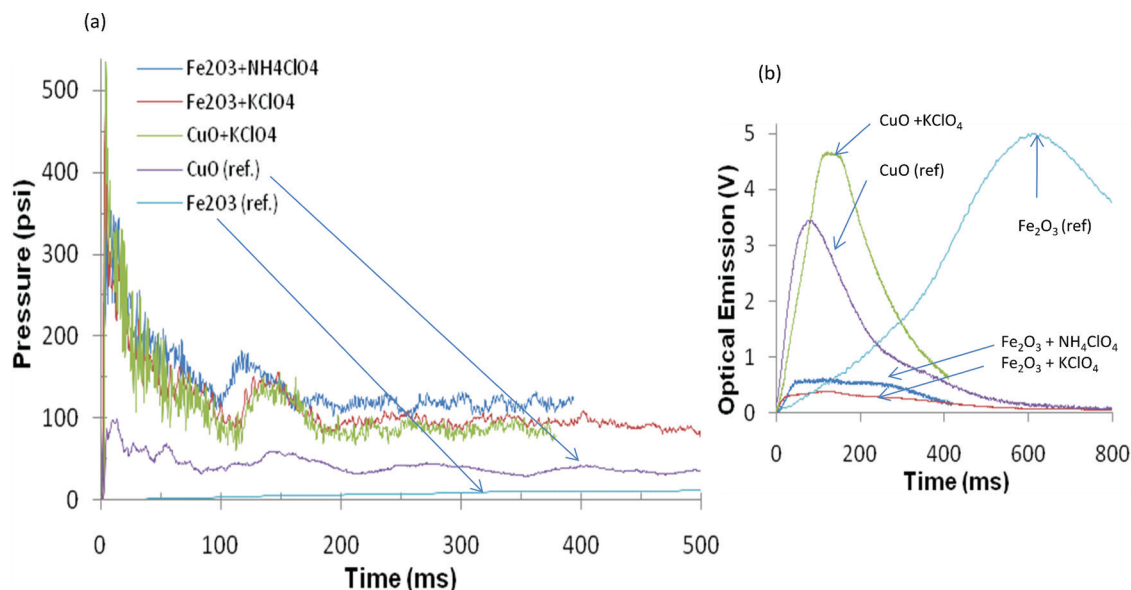


**Figure 5.** a) Simultaneous pressure and b) optical traces for various thermites as measured during combustion in a constant-volume pressure cell. All pressure traces show a rapid rise, with the synthesized perchlorate-included oxidizers significantly outperforming the reference materials CuO and Fe<sub>2</sub>O<sub>3</sub>. The optical traces for CuO-containing mixtures show an intense rise to a peak, followed by decay. The Fe<sub>2</sub>O<sub>3</sub>-containing mixtures, on the other hand, exhibit less-intense optical signals, and a “tail” lasting several hundred microseconds. All thermites were weighed stoichiometrically, assuming complete conversion to Al<sub>2</sub>O<sub>3</sub>. The elemental molar ratio in the synthesized oxidizers is [Cu/K] = [Fe/K] = [Fe/N] = 1/2.

We have recently argued that the pressurization occurs as a result of rapid oxidizer decomposition to release gaseous species, which can occur well before significant optical emission can be measured.<sup>[24]</sup> In oxidizers like CuO and Fe<sub>2</sub>O<sub>3</sub>, the gas is largely O<sub>2</sub>, however, the kinetics of the O<sub>2</sub> release differ due to the individual decomposition mechanisms. CuO can rapidly release O<sub>2</sub>, whereas Fe<sub>2</sub>O<sub>3</sub> cannot, due to the formation of FeO, which essentially traps O<sub>2</sub> in the condensed phase. In the current work, the synthesized oxidizers show the same relative behavior as an Al/CuO thermite; a rapid pressure signal followed by a prolonged optical signal. Therefore, we argue that the perchlorates burn by similar mechanisms. The mixture ignites, and the exothermic reaction rapidly drives the decomposition

of the oxidizer to pressurize the system, then the remainder of the fuel continues to burn in a pressurized, oxygenated environment. In the case of a perchlorate, several other gaseous species (K, Cl, N<sub>2</sub>, etc.) can form during the decomposition, and the formation of these gaseous species can greatly enhance the peak pressure, while also aiding in the convective energy transport throughout the thermites.

Direct comparison of the combustion of Al/(CuO+KClO<sub>4</sub>) and Al/(Fe<sub>2</sub>O<sub>3</sub>+KClO<sub>4</sub>) shows that the CuO system has a higher pressurization rate by about a factor of two, which is consistent with the idea that CuO decomposition contributes to the pressurization more than Fe<sub>2</sub>O<sub>3</sub> does.<sup>[25]</sup> By comparing the optical signals between the two systems, we see qualitative differences in the results. For the CuO system, the optical emission rises and falls, with a burn time (at full-width half-maximum) of ≈190 μs. In fact, both Al/CuO and Al/(CuO+KClO<sub>4</sub>) have similar burn times, which suggests that in both cases the burning is rate-limited by the aluminum fuel. For the Fe<sub>2</sub>O<sub>3</sub> system, however, the observed plateau in the optical emission suggests that the combustion occurs in two steps. We speculate that some of the oxidizer in the Fe<sub>2</sub>O<sub>3</sub> remains trapped as FeO, and thus the combustion ultimately is rate-limited by the oxidizer. The assignment of a burning time is somewhat ambiguous due to the plateau seen in the optical emission, however, it is characteristically longer than the CuO systems.

The reactivity of the MIC mixture could be tailored by varying the constituent content in the composite oxidizer particles. In particular, the metal oxide was thickened by increasing the ratio of the metal oxide precursor during the process of aerosol synthesis. This was done for both CuO+KClO<sub>4</sub> and Fe<sub>2</sub>O<sub>3</sub>+KClO<sub>4</sub>, and the pressure measurements are compared in Table 2. Not

**Table 1.** Measurements of the peak pressure and rise time for thermites prepared with the perchlorate-included systems relative to commercially available CuO. The pressurization rate is an accepted indicator of relative reactivity, and the results show a large enhancement in the reactivity for all synthesized oxidizers. All oxidizers were mixed with Al, and were prepared stoichiometrically assuming complete conversion to Al<sub>2</sub>O<sub>3</sub>. The elemental molar ratio in the synthesized oxidizers is [Cu/K] = [Fe/K] = [Fe/N] = 1/2. Typically a 25 mg sample was loaded in a 13 mL cell for the measurement.

Oxidizer (w/Al, φ = 1)	P <sub>max</sub> [psi]	Rise Time [μs]	Pressurization Rate [psi μs <sup>-1</sup> ]
(CuO+KClO <sub>4</sub> )	534	1.5	356
(Fe <sub>2</sub> O <sub>3</sub> +KClO <sub>4</sub> )	495	2.4	206
(Fe <sub>2</sub> O <sub>3</sub> +NH <sub>4</sub> ClO <sub>4</sub> )	389	3.3	117
CuO (ref.)	98	10.4	9.4
Fe <sub>2</sub> O <sub>3</sub> (ref.)	13	800	0.017

**Table 2.** Effect of changing the relative amount of metal oxide/perchlorate on thermite reactivity. Typically a 25 mg sample was loaded in a 13 mL cell for the measurement.

Oxidizer (w/Al, $\phi = 1$ )	Molar ratio	$P_{\max}$ [psi]	Pressurization rate [psi $\mu\text{s}^{-1}$ ]
(CuO+KClO <sub>4</sub> )	[Cu/K] = 1/2	534	356
(CuO+KClO <sub>4</sub> )	[Cu/K] = 2/1	279	112
(Fe <sub>2</sub> O <sub>3</sub> +KClO <sub>4</sub> )	[Fe/K] = 1/2	495	206
(Fe <sub>2</sub> O <sub>3</sub> +KClO <sub>4</sub> )	[Fe/K] = 2/1	240	97

surprisingly, the pressurization rate decreases as the less reactive metal oxide is thickened, and provides a simple method for tuning the thermite reactivity.

Experiments were conducted at high heating rates ( $\approx 5 \times 10^5 \text{ K s}^{-1}$ ) on 70- $\mu\text{m}$  diameter platinum wires to measure the ignition temperature of the thermites formulated with nanoaluminum and the synthesized composite oxidizer mixture. Based on the average of three repeated shots, the measured ignition temperatures of Al/(Fe<sub>2</sub>O<sub>3</sub>+KClO<sub>4</sub>) and Al/(CuO+KClO<sub>4</sub>) thermite are 1105 K and 1087 K, respectively, which are significantly lower than that of their corresponding single metal oxide thermite, i.e., >1500 K of Al/Fe<sub>2</sub>O<sub>3</sub>, >1200 K of Al/CuO.

Figure 6 gives sequential snapshots of Al/(Fe<sub>2</sub>O<sub>3</sub>+KClO<sub>4</sub>) and Al/(CuO+KClO<sub>4</sub>) burning on a wire under fast heating captured by the high-speed digital camera. Both of the perchlorate-containing thermites show much more violent reaction than that of Al/CuO (commercial) as obviously seen from the images; this indicates much faster energy release and pressurization rate for the perchlorate-containing thermites.

Our previous work showed that a clear correlation exists between O<sub>2</sub> release from the oxidizer and the overall reactivity of the formulated nano-thermite, i.e., high thermite reactivity can be reasonably attributed to the strong oxygen release of the oxidizer.<sup>[25]</sup> In this work, time-resolved mass spectrometry was conducted to study the O<sub>2</sub> release of the synthesized perchlorate-encapsulated composite oxidizer. O<sub>2</sub> peak intensity as a function of time obtained from flash heating along with a comparison of commercial Fe<sub>2</sub>O<sub>3</sub> nanopowder and synthesized (Fe<sub>2</sub>O<sub>3</sub>+KClO<sub>4</sub>) was plotted and shown in Figure 7. Not surprisingly, much higher O<sub>2</sub> signal intensity was observed from Fe<sub>2</sub>O<sub>3</sub>+KClO<sub>4</sub> than from commercial Fe<sub>2</sub>O<sub>3</sub> nanopowder. Clearly, quick release of abundant oxygen contributed to the high reactivity in our current thermite. Further, the onset temperature of O<sub>2</sub> release from Fe<sub>2</sub>O<sub>3</sub>+KClO<sub>4</sub> ( $\approx 1045 \text{ K}$ ) is much lower than that of commercial Fe<sub>2</sub>O<sub>3</sub> nanopowder ( $\approx 1524 \text{ K}$ ), but close to that of KClO<sub>4</sub> ( $\approx 1070 \text{ K}$ ), which suggests that the dominant source of O<sub>2</sub> is the perchlorate. Similar results were also observed from CuO+KClO<sub>4</sub> and Fe<sub>2</sub>O<sub>3</sub>+NH<sub>4</sub>ClO<sub>4</sub> samples, which further confirmed the origin of the O<sub>2</sub>.

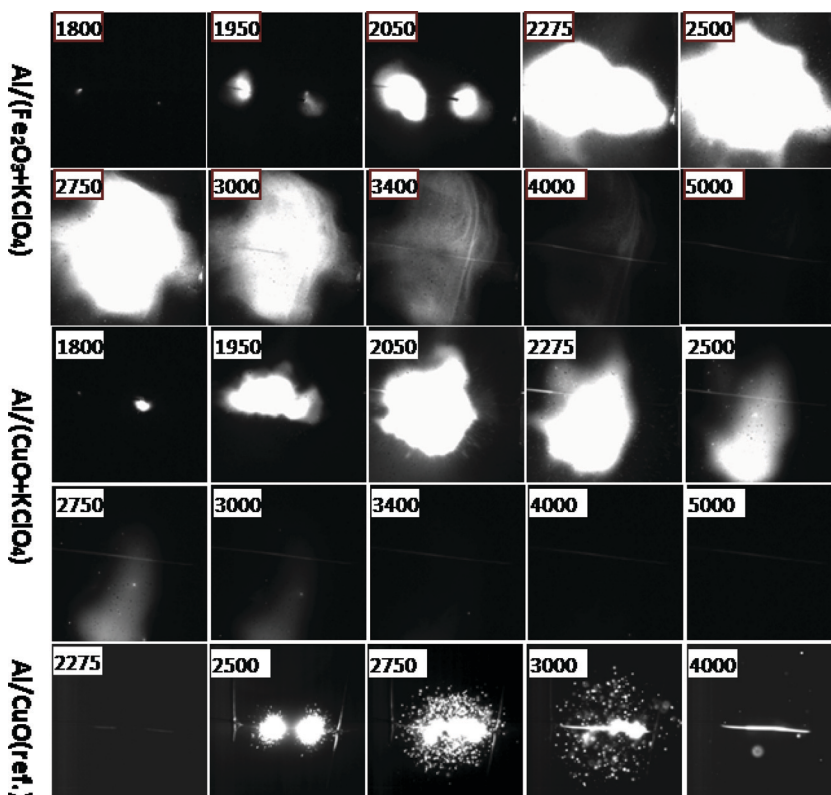


**Figure 6.** Sequential snapshots of Al/(Fe<sub>2</sub>O<sub>3</sub>+KClO<sub>4</sub>), Al/(CuO+KClO<sub>4</sub>), and Al/CuO (commercial) burning on fast-heating wire, as captured by high-speed video camera. The labeled numbers are time elapsed ( $\mu\text{s}$ ) after triggering.

### 3. Conclusion

Water-soluble and hygroscopic perchlorate salts, including KClO<sub>4</sub> and NH<sub>4</sub>ClO<sub>4</sub>, were successfully encapsulated by common metal oxides by using an aerosol synthesis approach. The unique microstructures of the composite oxidizer particles were characterized and structure evolution mechanisms discussed. Thermite samples formulated with nanofuel and synthesized oxidizers show a higher pressurization rate and peak pressure, a lower ignition temperature, and a faster and more intense O<sub>2</sub> release. High-speed imaging clearly shows a much more violent reaction than for traditional thermites. The results imply that a strategy of incorporating a very strong oxidizer within a milder oxidizer offers many advantages in controlling reactivity and enabling the use of a material that, due to long-term compatibility, would not normally be considered.

### 4. Experimental Section

**Materials:** Iron (III) nitrate nonahydrate (Fe(NO<sub>3</sub>)<sub>3</sub>·9H<sub>2</sub>O, > 98%), cupric nitrate trihydrate (Cu(NO<sub>3</sub>)<sub>2</sub>·3H<sub>2</sub>O, > 98%), ammonium perchlorate (NH<sub>4</sub>ClO<sub>4</sub>, 99.8%), potassium perchlorate (KClO<sub>4</sub>, = 99.5%), and reference CuO ( $\approx 50 \text{ nm}$ ) and Fe<sub>2</sub>O<sub>3</sub>

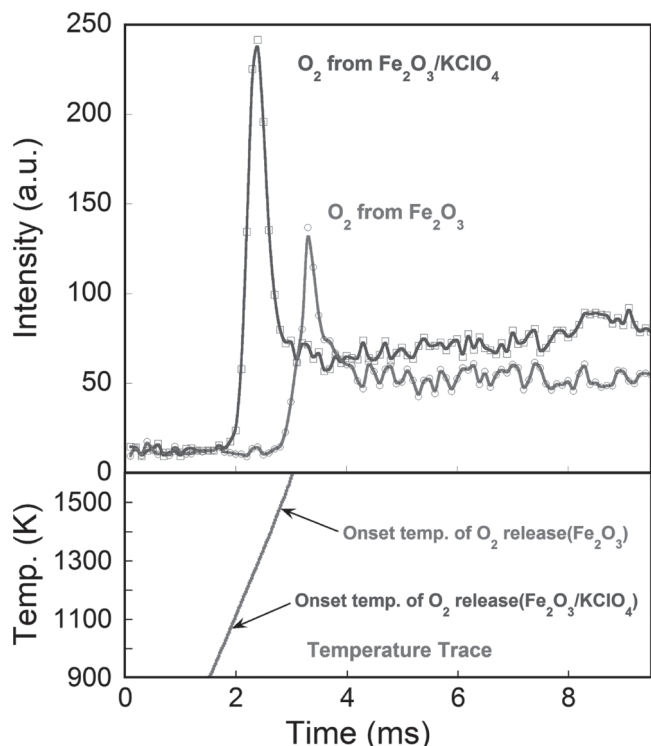


**Figure 7.** Temporal profile of oxygen release upon heating the synthesized composite oxidizer  $Fe_2O_3+KClO_4$  and commercial  $Fe_2O_3$  nanopowder. The heating pulse time was 3.0 ms.

(<50 nm) nanopowders were all purchased from Sigma-Aldrich and were used as received. The aluminum nanopowders used in the combustion test were obtained from the Argonide Corporation, and are designated as 50 nm ALEX by the supplier. The aluminum was found to be 70 wt% active as measured by thermogravimetric analysis (TGA).

**Aerosol Spray Drying and Pyrolysis:** The composite oxidizer particles were fabricated via a one-step, two-furnace temperature strategy in an aerosol setup, the scheme of which is shown in **Figure 8**. Aerosol droplets containing the dissolved precursors were generated by using a home-built pressure atomizer. The geometric mean diameter of the generated droplet, as measured by a laser aerosol spectrometer, is about 1  $\mu m$ . Droplets were passed through a diffusion dryer to remove most of the solvent, and then into tube furnaces to thermally decompose the included precursor salts and further densify the particle structure.

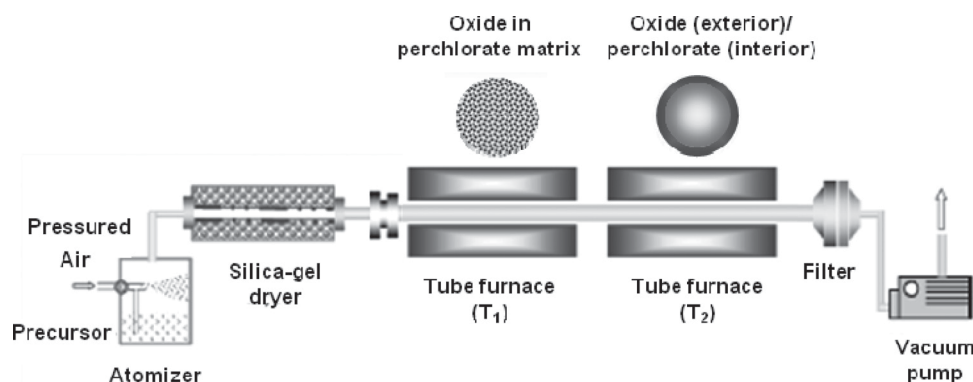


**Figure 8.** Aerosol spray drying/pyrolysis system for the fabrication of composite oxidizer particles.

Normal residence times were  $\approx 1$  second for a total gas flow rate of 3.5 L  $min^{-1}$ . Product particles were collected on a 0.4  $\mu m$  pore Millipore HTP membrane filter (housed in a stainless-steel holder and covered by a heating tape to prevent recondensation of solvent vapor. Typical product yields exceeded 50%.

**Thermite Sample Preparation:** The MIC sample powders were prepared by first weighing out the fuel and oxidizer and adding the contents to a ceramic crucible. Approximately 10 mL of hexane was then added, and the mixture was sonicated in an ultrasonating bath for 20 min to ensure intimate mixing. The hexane was then allowed to evaporate in air and then the samples were placed in a furnace at 100  $^{\circ}C$  for a few minutes to remove any remaining hexane. The powder was then very gently broken apart with a spatula until the consistency for each sample was that of a loose powder.

**Simultaneous Pressure and Optical Characterization of Reactivity:** The reactivity of MICs is typically reported as a relative value, due to the current lack of fundamental understanding of the reaction mechanism. Two common methods for measuring the reactivity of MICs are to combust the sample and measure the linear burning rate, and also to combust the material in a constant-volume cell and measure the pressurization rate. The flame velocity and pressurization rate have been shown to correlate with each other, however, the correlation is not quantitative. In this work, the pressurization rate from combustion in a small volume cell has been used to characterize the reactivity of the burning material. Since this is a relative measurement, a reference oxidizer (CuO) is shown with the data as a comparison. In a typical pressurization rate measurement in our experiment, a fixed mass (25 mg) of the sample powder was placed inside a constant-volume ( $\approx 13$  mL) pressure cell, and a nichrome wire coupled to an external power supply was placed in contact with the top of the powder, which served as an ignition source through resistive heating of the wire. A piezoelectric pressure sensor was employed in series with an in-line charge amplifier and a signal conditioner, and the resultant voltage trace upon ignition was captured by a digital oscilloscope. The pressurization rate ( $dP/dt$ ) was calculated by converting the voltage rise to pressure (1 mV = 0.237 psi), and dividing by the rise time in microseconds. Three repeated shots were performed for each sample for the average pressurization rate. The optical emission was simultaneously collected using a lens tube assembly, containing a planoconvex lens ( $f = 50$  mm), and a photodetector to collect the broadband emission.

**Time-Resolved Mass-Spectrometry Measurement of the Oxygen Release of the Oxidizers:** The recently developed temperature-jump/time-of-flight mass spectrometer (T-Jump/TOFMS) was used to characterize the reactivity of the nanocomposites. Typically, the T-Jump filament (Pt wire, length  $\approx 12$  mm, diameter  $\approx 76$   $\mu m$ ) was coated with a thin layer of sample powder (< 0.03 mg) which could be heated up to ca. 1800 K at a heating rate  $\approx 5 \times 10^5$  K  $s^{-1}$ . The filament was replaced after each heating event. From the current and voltage trace, a resistivity measurement can be obtained and related to the instantaneous temperature of the

filament, which can be mapped against the mass spectra. Time-resolved mass spectra combined with temperature information were then used for characterization of nanocomposite thermite reactions. A detailed experimental description of T-Jump/TOFMS can be found in our previous papers.<sup>[25,26]</sup>

**Simultaneous Fast-Heated Ignition Wire Test and High-Speed Imaging:** The T-Jump technique was coupled with a photomultiplier tube (PMT) setup for the measurement of the optical emission. The ignition temperature of the thermite sample reaction was obtained from the correlated emission signal with temperature profile of the T-Jump filament. The experiments used the same T-Jump wire in the T-Jump/TOFMS except for those performed at atmospheric pressure. A detailed experimental description can be found in our previous papers.<sup>[25,26]</sup> High-speed digital video imaging of sample burning was conducted with a Vision Research Phantom® v9.1 digital camera, which has a maximum resolution of 1632 × 1200 and maximum frame rate of 153846 fps at 96 × 8 resolutions.

## Acknowledgements

Support for this work comes from the Army Research Office and the Defense Threat Reduction Agency, and the authors appreciate microscopy support through the University of Maryland Nanocenter.

Received: March 2, 2011

Published online: November 7, 2011

- 
- [1] C. Rossi, K. Zhang, D. Estève, P. Alphonse, P. Thailhades, C. Vahlas, *J. Microelectromech. Syst.* **2007**, *16*, 919.
- [2] M. Petrantonio, C. Rossi, V. Conédéra, D. Bourrier, P. Alphonse, C. Tenailleau, *J. Phys. Chem. Solids* **2010**, *71*, 80.
- [3] K. B. Plantier, M. L. Pantoya, A. E. Gash, *Combust. Flame* **2005**, *140*, 299.
- [4] S. Majumdar, G. B. Kaleb, I. G. Sharma, *J. Alloy Compd.* **2005**, *394*, 168.
- [5] M. E. Brown, S. J. Taylor, M. J. Tribelhorn, *Propell. Explos. Pyrotech.* **1998**, *23*, 320.
- [6] A. N. Pivkina, Y. V. Frolov, D. A. Ivanov, *Combust. Explos. Shock Waves* **2007**, *43*, 51.
- [7] J. L. Cheng, H. H. Hng, H. Y. Ng, P. C. Soon, Y. W. Lee, *J. Phys. Chem. Solids* **2010**, *71*, 90.
- [8] C. E. Aumann, G. L. Skofronick, J. A. Martin, *J. Vac. Sci. Technol. B, Microelectron. Process. Phenom.* **1995**, *13*, 1178.
- [9] B. W. Asay, S. F. Son, J. R. Busse, D. M. Oschwald, *Propell. Explos. Pyrotech.* **2004**, *29*, 216.
- [10] B. S. Bockmon, M. L. Pantoya, S. F. Son, B. W. Asay, J. T. Mang, *J. Appl. Phys.* **2005**, *98*, 064903.
- [11] M. L. Pantoya, V. I. Levitas, J. J. Granier, J. B. Henderson, *J. Propul. Power* **2009**, *25*, 465.
- [12] S. Apperson, R. V. Shende, S. Subramanian, D. Tappmeyer, S. Gangopadhyay, Z. Chen, K. Gangopadhyay, P. Redner, S. Nicholich, D. Kapoor, *Appl. Phys. Lett.* **2007**, *91*, 243109.
- [13] S. Subramaniam, S. Hasan, S. Bhattacharya, Y. Gao, S. Apperson, M. Hossain, R. V. Shende, S. Gangopadhyay, P. Redner, D. Kapoor, S. Nicholich, *Proc. Mater. Res. Soc. Symp.* **2006**, *896*, 0896-H01-05.1.
- [14] K. Zhang, C. Rossi, G. A. A. Rodriguez, C. Tenailleau, P. Alphonse, *Appl. Phys. Lett.* **2007**, *91*, 113117.
- [15] S. H. Kim, M. R. Zachariah, *Adv. Mater.* **2004**, *16*, 1821.
- [16] J. D. Ferguson, K. J. Buechler, A. W. Weimer, S. M. George, *Powder Technol.* **2005**, *156*, 154.
- [17] G. M. Dutro, R. A. Yetter, G. A. Risha, S. F. Son, *Proc. Combust. Inst.* **2009**, *32*, 1921.
- [18] S. H. Fischer, M. C. Grubelich, Proc. 24th Int. Pyrotechnics Seminar, Monterey, CA, **Jul. 1998**, 1–6.
- [19] S. Jain, M. S. Nandagopal, P. P. Singh, K. K. Radhakrishnan, B. Bhattacharya, *Defense Sci. J.* **2009**, *59*, 294.
- [20] H. Laucht, H. Bartuch, D. Kovalev, Proc. 7th Int. Symp. Exhib. Sophisticated Car Occupant Safety Syst., **2004**, 12–16.
- [21] E. W. Fournier, B. B. Brady, *J. Propul. Power* **2005**, *21*, 937.
- [22] A. Prakash, A. V. McCormick, M. R. Zachariah, *Nano Lett.* **2005**, *5*, 1357.
- [23] K. S. Martirosyan, L. Wang, A. Vincent, D. Luss, *Nanotechnol.* **2009**, *20*, 405609.
- [24] K. Sullivan, M. R. Zachariah, *J. Propul. Power* **2010**, *26*, 467.
- [25] L. Zhou, N. Piekielek, S. Chowdhury, M. R. Zachariah, *J. Phys. Chem. C* **2010**, *114*, 14269.
- [26] L. Zhou, N. Piekielek, S. Chowdhury, M. R. Zachariah, *Rapid Commun. Mass Spectrom.* **2009**, *23*, 194.
-